Macromolecules
ARTICLE

Macromolecules **2009**, *42*, 5395–5401 **5395**
DOI: 10.1021/ma900754v

Segmental Dynamics of Semicrystalline Poly(vinylidene fluoride) Nanorods

Jaime Martín and Carmen Mijangos

Instituto de Ciencia y Tecnología de Polímeros, CSIC. Juan de la Cierva 3, Madrid 28006, Spain

Alejandro Sanz, Tiberio A. Ezquerra, and Aurora Nogales*

Instituto de Estructura de la Materia, CSIC. Serrano 121, Madrid 28006, Spain

Received April 7, 2009; Revised Manuscript Received June 4, 2009

ABSTRACT: The dynamics of a semicrystalline poly(vinylidene fluoride) (PVDF) confined within alumina templates of cylindrical nanopores is studied by means of dielectric spectroscopy. In this study we demonstrate how the counterbalance between spatial confinement and interfacial interactions controls at the nanometer level the dynamic and semicrystalline structure of the polymer. A strong deviation of the relaxation behavior of PVDF embedded within the nanopores is observed as compared to that of the bulk. In particular, the dielectric measurements reveal, for pore sizes of the order of 20 nm, the existence of a highly constrained relaxation associated with the polymer−alumina interfacial layer.

Introduction

Understanding the behavior of systems at the nanometer scale is a crucial step to the development of nanotechnology. In the case of polymer physics, the confinement of molecules to dimensions that are in the range of their molecular sizes implies severe changes of the physical behavior. Dramatic finite size effects can be observed, for example, on the polymer dynamics as well as on the crystallization behavior.

Crystallization can be considered as the most common self-assembly process in nature.[1] In polymers, the crystallites formed are typically thin in one dimension (in the order of about 10 nm) and of comparatively large lateral extent, leading to micrometer-scale superstructures like, for example, spherulites.[2] Several approaches have been applied to study the role of confinement on crystallization. The crystallization of polymer thin films supported onto a substrate has been deeply investigated due to their applications in fabricating microelectronic systems. It has been shown that, even for highly crystallinity systems in bulk, the crystallization can be hindered when the film thickness is small enough.[3] Also, confinement effects on crystallization have been studied within block copolymer microdomains, demonstrating that the finite size of the domains affects drastically the crystallization kinetics.[4] In this case, crystallization is initiated homogeneously (in contrast to the general trend in bulk polymers), and the observed crystallization kinetics are first-order rather than the Avrami behavior conventionally observed during polymer crystallization. Also, the crystal orientation into the lamellar and cylindrical domains of a block copolymer has been found to have a strong dependence with the crystallization temperature and the confinement dimensions.[5−8] For example in poly(ethylene oxide)-*b*-polystyrene diblock copolymer systems a strong influence of the confinement on the crystal growth has been reported.[6−8]

Molecular dynamics also changes dramatically when polymer chains are confined to the scale of several nanometers. The segmental dynamics is affected upon confinement. The change from the glass behavior to that of a supercooled liquid in the temperature region around the glass transition (T_g) is strongly affected by confinement. In bulk, a dramatic increase of the characteristic relaxation time τ is observed as the temperature is lowered (α-relaxation). This can be interpreted as resulting from a cooperative behavior of the relevant molecular motions characterized by a characteristic length scale ξ which increases with decreasing temperature.[9] In the vicinity of T_g, this length scale is expected to be in the order of magnitude of few nanometers, specifically from 1 to 3 nm depending on the rigidity of the polymer chain.[10] Physically, confining a glass former in a geometry of characteristic dimension r should affect its behavior when the finite size r is of the same order as ξ. These ideas have motivated experiments aiming to detect the size ξ by tuning the confinement length. Among these experiments, confinement of polymers in pores,[11] thin films,[12] and nanocomposites[13−15] has been reported. However, unambiguous evidence on the nature and size of these heterogeneities has not been found.[16] In general, at this nanometer level, confinement might compete with surface interaction effects.[17,18] Recently, it has been shown that confinement affects not only segmental dynamics but also the chain dynamics of polymers, where an unexpected enhancement of the flow and a reduction in intermolecular entanglements have been found.[19]

In recent time, electrochemically fabricated porous materials have been used as confining systems with very well-defined geometry for polymer crystallization studies. It is well-known that high surface energy solids such as metal oxides are wettable by almost all low surface energy systems like polymer melts. When a polymer melt is deposited on top of a porous anodic aluminum oxide (AAO) template, the polymer wets the pores. Depending on the size of the pore, the annealing temperature, and the spreading coefficient for the given polymer/alumina system, two wetting regimes (partial and total wetting) are observed, giving rise to two different polymeric nanostructures inside the pores (nanorods or nanotubes).[20−22] The effect of the two-dimensional (2D) confinement imposed by the pores on the crystallization of polymers has been reported.[23−27]

*To whom correspondence should be addressed.

© 2009 American Chemical Society
Published on Web 06/24/2009

Steinhart et al. have shown that the curvature of the confinements can affect the crystal orientation of polymers.[24,25] By studying the orientation of crystals of poly(vinylidene fluoride) under cylindrical confinements, they have observed that the crystallites grow preferentially in the direction of minimum curvature on the surfaces of cylindrical confinements. Also, recent studies in polyethylene confined within porous alumina membranes demonstrate that the frustration driven by the nanoscopic constrained geometry induced a nucleation-dominant crystallization. A specific orientation of linear PE crystals in nanocylinders was found when they were crystallized slowly; the *b*-axis of orthorhombic PE crystals was parallel to the long cylindrical axes of the nanopores, while *a*- and *c*-axes were nearly on the plane perpendicular to the cylindrical axes.[23] Similar studies on the segmental dynamics of polymers embedded within the alumina membranes are still scarce.

PVDF is a semicrystalline polymer which can be infiltrated in AAO templates producing either nanotubes or nanorods depending on the pore size and on the conditions of the infiltration.[28] In this work three different PVDF nanorods were prepared by using AAO templates with 60, 35, and 20 nm of pore diameter and 100 μm in pore length. In this work we report on the effect that the 2D confinement imposed by the cylindrical pores produces in the segmental dynamics of a semicrystalline poly(vinylidene fluoride). We observed a strong deviation in the relaxation behavior of the amorphous phase of poly(vinylidene fluoride) (PVDF) embedded within self-ordered porous aluminum oxide templates[29] as compared to that of the bulk, resulting in the appearance of a highly constrained relaxation.

Experimental Section

Samples. *Anodic Aluminum Oxide Templates*. The ordered AAO templates with average diameter values of 35 and 60 nm were prepared by a two-step anodization process of aluminum using oxalic acid as electrolyte at 40 V as described elsewhere.[29] On the other hand, the AAO with 20 nm in diameter pores was prepared anodizing aluminum in 10 wt % sulfuric acid solution at 19 V.[30] All templates were 100 μm in length. The templates are comprised of a hexagonal array of parallel cylindrical pores oriented perpendicularly to the surface of the template. The morphology of the AAOs was characterized by a scanning electron microscope (SEM, Philips XL-30 ESEM).

PVDF Nanorods. Commercially available PVDF (Aldrich Ltd., M_w = 180 000 g/mol, M_n = 71 000 g/mol) was used for our experiments. For the preparation of the PVDF nanorods, several polymer pellets were placed onto the AAO templates in order to carry out the infiltration by the "precursor film" infiltration method.[28] In this method, a polymeric liquid precursor film spreads over the whole surface of the AAO template, pore walls included. Since the thickness of the precursor film is larger that the pore radius, a complete filling of the nanopores is achieved. The AAO with the PVDF pellets were then annealed at 240 °C under a nitrogen atmosphere for 45 min. After the infiltration process, the samples were quenched under ice−water. In order to force the separated crystallization of each individual nanorod, the residual PVDF film located on the AAO surface, which connected the nanorods, was removed with a blade. Finally, the nanorods were again molten at 240 °C and quenched in ice−water.

Differential Scanning Calorimetry. A differential scanning calorimeter (DSC) (Perkin-Elmer DSC-7) was used for thermal characterization of samples. Heating runs at 10 °C/min were accomplished under a constant flow of nitrogen and using a cryogenic bath of liquid nitrogen to enable temperature scanning from 0 °C.

Dielectric Spectroscopy. Dielectric spectroscopy (DS) measures the complex dielectric permittivity $\varepsilon^* = \varepsilon' - i\varepsilon''$ as a function of frequency, where ε' is the dielectric constant and ε'' is the dielectric loss. Infiltrated PVDF in alumina templates were placed between two electrodes of 1 cm diameter with the nanorod axis perpendicular to the electrodes. Dielectric loss measurements $\varepsilon'' = \mathrm{Im}(\varepsilon^*)$ were performed over a broad frequency window, $10^{-1} < F\,(\mathrm{Hz}) < 10^7$ by means of a Novocontrol system integrating a dielectric interface (ALPHA) and a temperature control by nitrogen jet (QUATRO) with a temperature error, during every single sweep in frequency, of 0.1 K. The analysis of the results was carried out by means of the Novocontrol program WinFit.

Small-Angle X-ray Scattering. Small-angle X-ray scattering (SAXS) experiments have been accomplished by a NanoSTAR-U system by Bruker using Cu Kα radiation (λ = 0.154 nm) equipped with a three-pinhole collimation system, cross-couple Göbel mirrors, and a Hi-Star multiwire area detector. The SAXS data have been corrected for background scattering by considering the absorption coefficient. Reciprocal space calibration has been done using collagen as standard.

Temperature-Resolved Wide-Angle X-ray Scattering. Wide-angle X-ray scattering (WAXS) measurements were performed at the BM16 beamline of the European Synchrotron Radiation Facility (ESRF), Grenoble, France. BM16 uses radiation from one of the ESRF bending magnets with a critical energy of 19.6 keV. The optics is based on a flat vertically collimating mirror, a double-crystal monochromator Si(111), and a toroidal mirror. The optics is designed to provide an optimized flux and focal spot in the 6−17 keV energy range. In the present case an energy of 12.4 keV corresponding to a wavelength of $\lambda = 0.1$ nm was used. The WAXS detector was a CCD camera PI SCX90-1300 from Roper Scientific. The active surface is 65 × 65 mm^2 and has 1242 × 1152 pixels. The CCD detector is mounted on a supporting arm attached to a one circle goniometer rotation unit RV240PE from Newport.[31] The temperature control during the experiment was obtained by a Linkam hot stage.

The small- and wide-angle X-ray scattering experiments were performed in transmission, with the nanocylinder approximately parallel to the incident beam.

Results and Discussion

Figure 1 shows scanning electron microscopy (SEM) images of the PVDF nanorods after dissolving the alumina template (right panel) and of the AAO templates before infiltration (left panel). The different samples have been labeled as reported in Table 1.

The wide-angle X-ray scattering (WAXS) patterns of the bulk sample and of the samples infiltrated in alumina pores are shown in Figure 2. For the bulk, sample B, the characteristic α crystalline phase of PVDF is recognized.[24] The α phase has four major reflections, marked on the upper panel of Figure 2. It is clear from the WAXS patterns that the confined samples present lower crystallinity. It is interesting to note that, when comparing the WAXS corresponding to samples B and P35 sample, the last one exhibits only two out of the four major reflections of the α phase of PVDF. The reflections observed are the 110 and the 020 reflections of the α phase. However, the 021 reflection is absent in this sample. This result is in accordance with that obtained by Steinhart et al.,[24] who proposed that in this range of pore sizes the morphology is dominated by crystals with a $\langle hk0\rangle$ direction aligned with the long axes of the pores. Only for such an orientation are the lamellae able to grow straight along the pores. Lamellae whose crystals are oriented with a $\langle hkl\rangle$ direction with nonzero *l* index parallel to the pore axis cannot grow. These two reflections are also observed in the nanorods infiltrated in 20 nm pores superimposed to the alumina contribution.

The partial hindering of crystallization in the confined PVDF samples is also revealed in the calorimetric experiments, especially in the cooling runs, where for the confined samples only a slight and broad crystallization peak is observed, located at temperatures lower than that of the bulk sample (Figure 3). For the

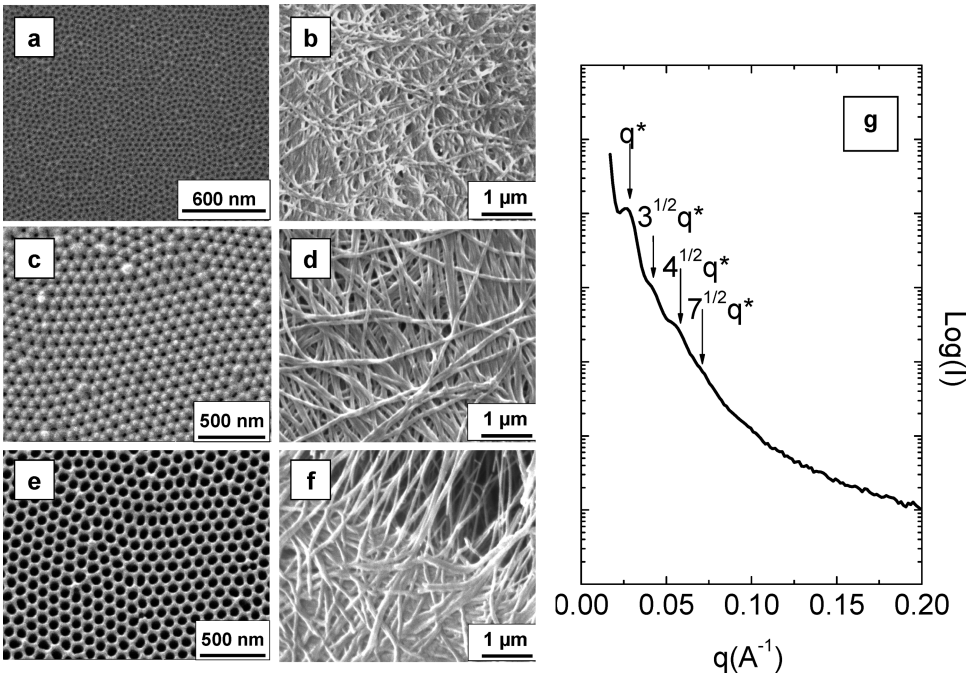

Figure 1. SEM micrographs of the surfaces of AAO templates with pores of 20 nm (a), 35 nm (c), and 60 nm (e) in diameter and the PVDF nanofibers obtained respectively from them (b, d, and f). (g) Small-angle X-ray scattering obtained from the 20 nm AAO template. q^* indicates the position of the main maximum.

Table 1. Nomenclature Applied to the Studied Samples and D and T_0 Parameters According to the VFT Equation (Eq 3)[a]

label		D	T_0 (K)
B	bulk PVDF	7.5	177
P60	PVDF confined in 60 nm in diameter AAO pores	10.5	151
P35	PVDF confined in 35 nm in diameter AAO pores	11.3	147
P20	PVDF confined in 20 nm in diameter AAO pores		

[a] VFT parameters for the 20 nm samples have not been included since the α-relaxation for this sample is very weak and cannot be resolved in a wide enough temperature range to obtain reliable fittings.

sample confined into 20 nm pores it was not possible to obtain reliable DSC traces.

Dynamically, strong differences are observed when comparing the α relaxation of the bulk with that of the confined samples. The dielectric response of the bulk sample (Figure 4) is characterized by two main relaxation processes labeled as α and α_c in order of increasing temperature (or decreasing frequencies). The α process is related to the cooperative segmental motions appearing in the supercooled liquid, whereas the α_c relaxation is attributed to molecular motions in the crystal.[32] In the studied frequency window and at temperatures between −50 and 30 °C the most prominent relaxation in the dielectric spectrum of the bulk sample is the α relaxation. When comparing the bulk α relaxation with that of the confined samples, one may establish two cases, depending on the diameter of the pore. The extreme case of the P20 sample, where the polymer is confined into a 20 nm diameter cylinder, exhibits a dramatically different behavior to that of the bulk. The most prominent feature in the dielectric spectrum of P20 is a process appearing at low frequencies, indicating a much slower dynamics than that of the bulk α relaxation in a similar temperature range (see Figure 4). This effect is emphasized in Figure 5 where data for the dielectric relaxation at $T = -10$ °C of the bulk and the 20 nm pore sample are presented. Whereas the dielectric relaxation of the bulk is characterized by a maximum centered on $F = 10^4$ Hz, the main relaxation in the spectrum of the P20 sample at this temperature is centered

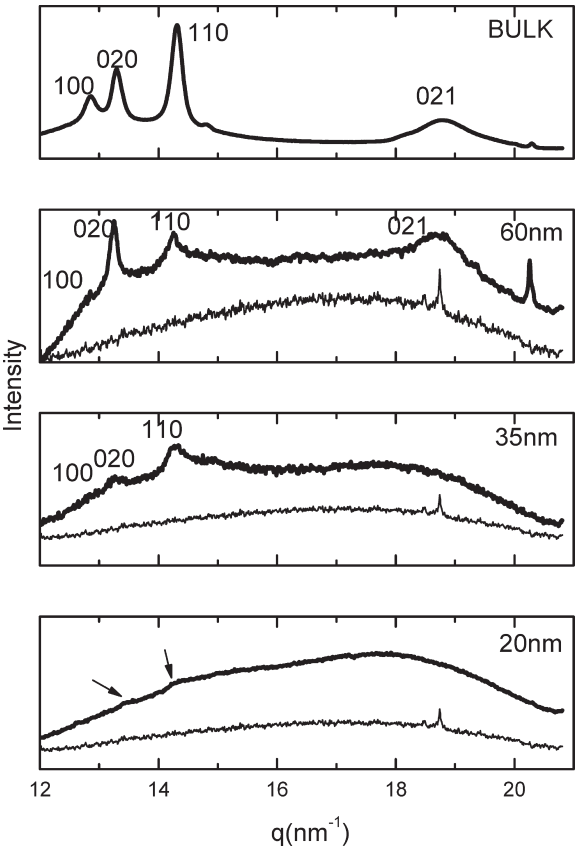

Figure 2. Wide-angle X-ray scattered intensity for PVDF in bulk and infiltrated in alumina pores of different diameters as indicated by the legends. Thin lines show the AAO template contribution. The numbers indicate the Miller indexes of the main reflections of the α phase of PVDF which have been indicated by arrows in the lower panel.

on 2 × 100 Hz, and it is much sharper that the bulk relaxation. Detailed analysis of the spectrum of the P20 sample reveals,

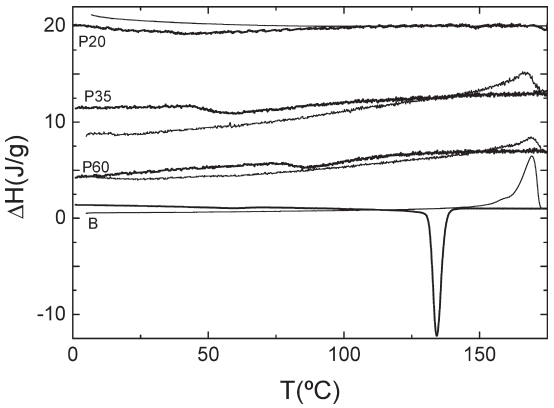

Figure 3. DSC scans of PVDF nanocylinders within alumina templates (thick lines, cooling runs; thin lines, heating runs, both at 10 °C/min). The curves were corrected by subtracting the contribution of the alumina (determined by reference measurements of empty membranes).

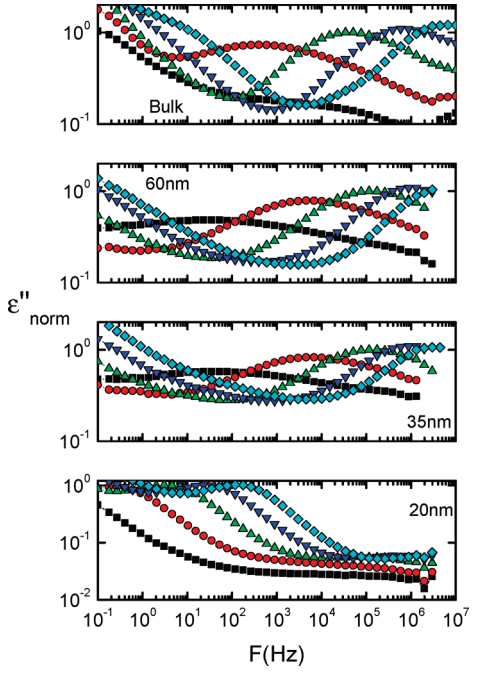

Figure 4. ε'' values as a function of frequency for selected temperatures: (■) −50, (●) −30, (▲) −10, (▼) 10, and (◆) 30 °C. The values have been normalized to the maximum at $T = -10$ °C. Labels inside the graphs represent the pore size.

however, that the usual α relaxation can still be observed in the form of a less intense maximum appearing in the region of high frequencies. For larger pores (P35 and P60 samples), the α relaxation appears at frequencies similar to that of the bulk sample, but subtle differences are also observed (Figure 4) which can be analyzed by using the Havriliak−Negami equations as reported elsewhere.[33] This formalism gives the following expression for the complex dielectric permittivity:

$$\varepsilon^* = \varepsilon_\infty + \frac{\varepsilon_0 - \varepsilon_\infty}{[1+(i\omega\tau_{HN})^b]^c} \quad (1)$$

where ε_0 and ε_∞ are the relaxed and unrelaxed dielectric constant value, respectively, τ_{HN} is the central relaxation time, and b and c are parameters which describe the symmetrical and asymmetrical broadening of the relaxation time distribution function, respectively. The mean relaxation time

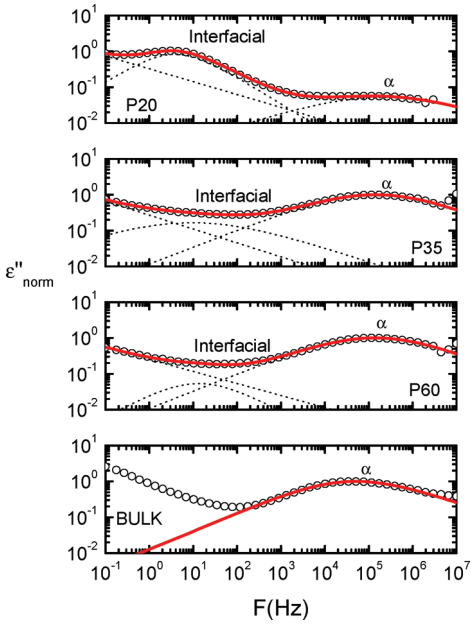

Figure 5. ε'' values as a function of frequency for the studied samples. The dotted curves in the P20, P35, and P60 samples indicate separate contributions from the α and interfacial relaxation, respectively. In the bulk samples it is possible to observe also the high-frequency tail of the α_c relaxation.

of the relaxation times distribution function is calculated through

$$\tau = \tau_{HN}\left[\sin\left(\frac{b\pi}{2+2c}\right)\right]^{-1/b}\left[\sin\left(\frac{bc\pi}{2+2c}\right)\right]^{1/b} \quad (2)$$

The difference $\Delta\varepsilon = \varepsilon_0 - \varepsilon_\infty$ is called the dielectric strength, and it is related to the amount of dipoles involved in the relaxation process and with the effective dipole moment. The results from this analysis are shown in Figure 6 as a function of temperature. Figure 7 illustrates the relaxation map of the PVDF samples in bulk and under confinement. In this figure, the mean relaxation time (τ), which is plot in a logarithmic scale versus the reciprocal temperature, exhibits the characteristic curvature described by means of the Vogel−Fulcher−Tamann equation (VFT):

$$\tau = \tau_0 \exp[DT_0/(T - T_0)] \quad (3)$$

The continuous lines in Figure 7 correspond to the fittings of the VFT equation to the experimental points with the D and T_0 values included in Table 1. The most prominent relaxation for samples B, P60, and P35 is the α relaxation, which exhibits a clear non-Arrhenius behavior. Although much less intense, the α relaxation is also present in the P20 sample and exhibits the same behavior with temperature than that of the P35 and P60 samples. The α relaxation in the confined samples with large pore diameter presents some differences when compared to that of the bulk samples. Its dependency with temperature is different, being faster at low temperatures. This enhancement of the dynamics at low temperatures for the samples confined in pores seems similar to that observed in polymers and low molecular weight liquids confined in glass pores[34,35] and in confined high molecular weight systems[18] although in the present case the fact that the polymer is semicrystalline can add up a new effect. It is known that the dynamics of the α relaxation is strongly affected by the presence of crystallinity.[33,36] The

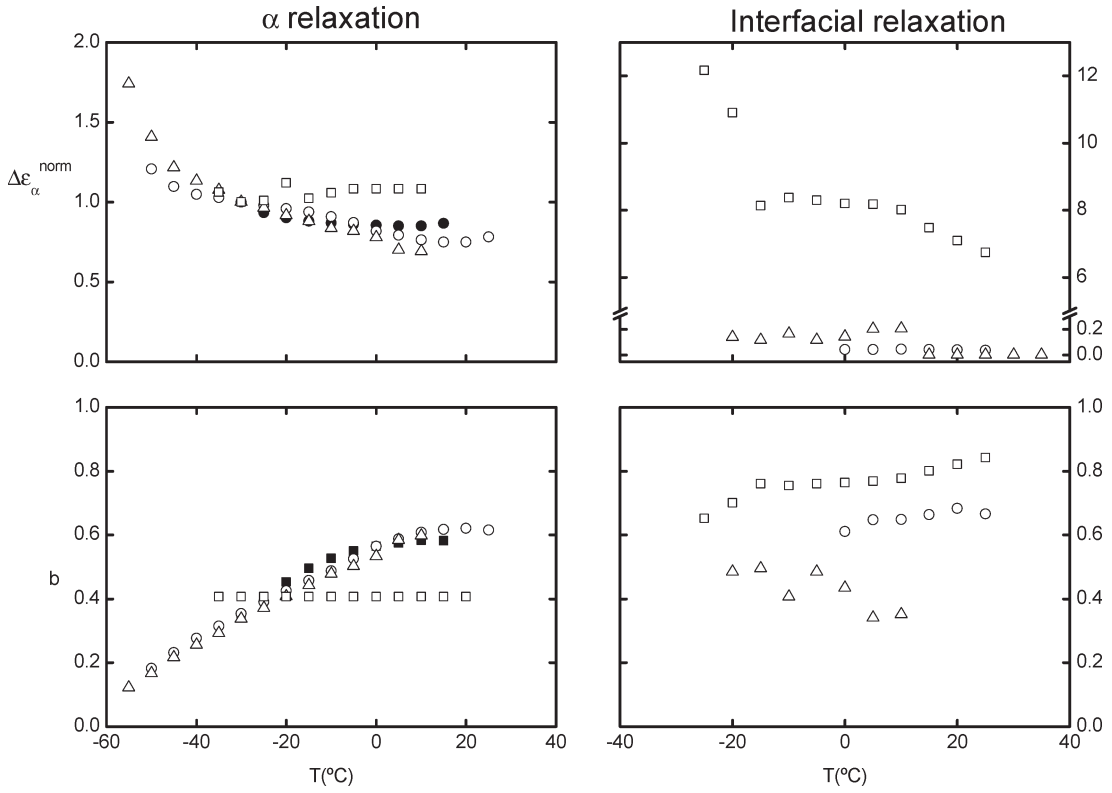

Figure 6. Variation with temperature of the dielectric strength ($\Delta\varepsilon$) and shape parameter (b) of the α and interfacial relaxations with temperature for the studied samples: (●) B, (○) P60, (Δ) P35, and (□) P20. For the sake of comparison, the dielectric strengths have been normalized to the value obtained for that of the α relaxation at $T = -30$ °C.

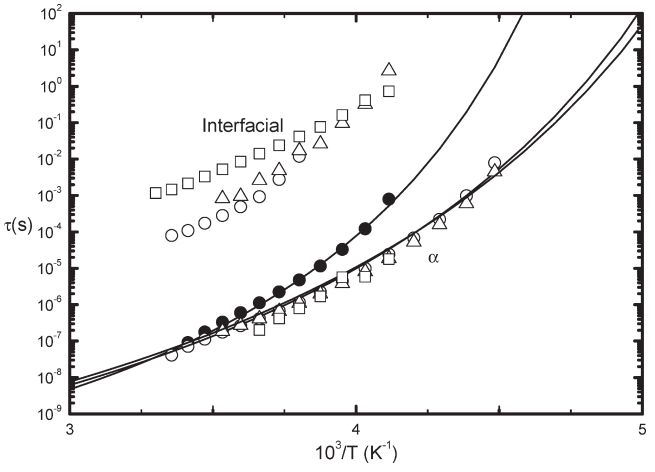

Figure 7. Dependence of the relaxation time (τ) of the observed relaxations, with the reciprocal temperature for the relaxations for the studied samples: (●) B, (○) P60, (Δ) P35, and (□) P20. Continuous lines are the best fittings to the VFT equation.

presence of crystals produces an increase of the α relaxation time and a broadening of the relaxation time distribution function.[24,33] As mentioned above, one of the confining effects observed in PVDF in the cylindrical pores of the AAO templates is a reduction the crystallinity. In this sense, it appears reasonable that the α relaxation of the confined systems is faster and the relaxation time distribution function narrower. The experimental results obtained support also this interpretation. In addition to the faster dynamics evidenced in the relaxation map (Figure 7), the values for the dielectric loss presented in Figure 4 show a narrower maximum corresponding to the α relaxation in the case of the samples confined in pores. This is especially obvious in the P60 and P35 samples. However, the fact that the most important relaxation in the sample confined in the smallest pore is slower than that of the bulk α relaxation has to be discussed considering that the molecular dynamics of polymers in confining geometries can always be influenced by the effect of the interaction with the internal pore surface.[17,37]

As observed by small-angle neutron scattering, X-ray reflectivity, and X-ray scattering among others techniques,[37−40] and predicted by simulation[41] when a polymer thin film is coated over a surface, there is a polymer region close to the surface where the chains are anisotropically coiled. Precisely, they are squashed parallel to the surface due to wall interaction. Furthermore, if the interaction between the surface and the polymer is attractive, there is a layer with a thickness of a few R_g, being R_g the radius of gyration, that has highly restricted mobility.[40] A reduced mobility layer has been observed by dielectric spectroscopy in aluminum-capped thin films of poly(ethylene terepthalate).[42] In the case studied here, additionally to the van der Waals forces that favors wettability, in the infiltrated PVDF, due to the electronegativity of the fluorine groups, hydrogen bonds can be created with the OH groups on the AAO surface, originating an attractive interaction between the alumina walls and the polymer chains.

On the other hand, simulations of polymer crystallization in thin films and in pores with attractive walls show that, for confinement in small volumes, the crystallization can be inhibited.[43,44] This result is in agreement with our calorimetric results, where, upon cooling, it is clearly seen that the crystallization peak shifts toward lower temperatures for polymers in the pores (Figure 3). Also, the same simulations predict that mainly the growth of flat-on lamellar crystals is favored as compared to the growth of edge-on lamellar crystals,[43,44] which is also consistent with our and previous[24] X-ray scattering observations (see Figure 2).

With all the above considerations a plausible explanation for the strongly restricted mobility observed in the P20 sample needs

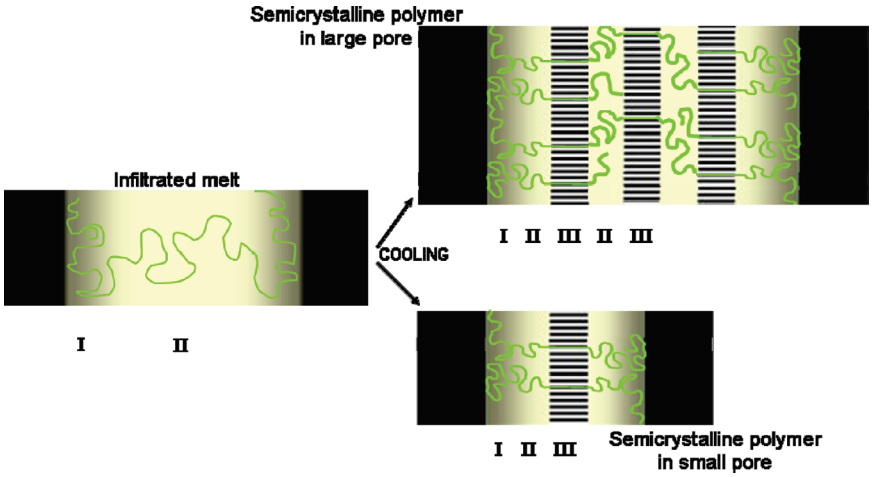

Figure 8. Scheme of the proposed model for layers with different mobility. During infiltration from the melt, an adsorbed layer (I) in contact with the walls is formed. Upon cooling, and depending on the pore size, one may find two situations: several PVDF crystals (III) aligned flat on with respect to the pore walls (large pore diameters) separated by amorphous layers (II) or a single PVDF lamella oriented also edge on (III). The amorphous phase in this latter case is mainly included in the adsorbed layer (I), and therefore, it relaxes in a particular way, as compared to the bulk relaxation.

to consider the nanostructure of PVDF. SAXS measurements in bulk PVDF shows that the nanostructure of the semicrystalline system consist of a stacking of lamellar crystals separated by the amorphous layer.[45] This stacking has a characteristic long period of ~12 nm with crystalline lamellar thicknesses of around 4 nm and interlamellar amorphous layers of 7−8 nm. In bulk PVDF, the observed α relaxation can be therefore associated with the interlamellar amorphous regions. But, where is the α relaxation observed in the nanopores coming from? By geometric considerations, and considering flat-on orientation of the lamellar crystals into the cylindrical pores, in the case of the 35 and 60 nm diameter pores, there would be enough space to grow at least two crystalline lamella. That means that there will be one or several interlamellar amorphous regions which, in principle, would be similar to those of the bulk. Accordingly, for the intermediate pore sizes, the observed α relaxation can be assigned to occur in these interlamellar amorphous regions having qualitatively similar behavior to the one of the bulk. However, for the extreme case of the 20 nm size pore, the space in the pore is not enough to accommodate more than one flat on lamellar crystal. Our relaxation measurements for the P20 sample would be compatible with the existence of a polymer amorphous layer in contact with the pore wall where the mobility is significantly reduced as compared to that of the bulk. Therefore, it is reasonable to assume that the lamellar crystal will tend to be located toward the center of the pore where the mobility is expected to be higher. These observations are summarized in the scheme presented in Figure 8.

Conclusions

By dielectric spectroscopy experiments we observe that the relaxation behavior of confined semicrystalline poly(vinylidene fluoride) (PVDF) within templates of cylindrical nanopores differs from that of the bulk polymer. In particular, for pore sizes of the order of 20 nm, the existence of a highly constrained relaxation is associated with the polymer−alumina interfacial layer. When the PVDF is confined to this level in alumina templates, most of the chains are located in the interfacial region, where the mobility is severely restricted, and because of that, crystallization is inhibited. The counterbalance between spatial confinement and interfacial interactions controls at the nanometer level the dynamic and semicrystalline structure of the polymer.

Acknowledgment. The authors acknowledge the financial support from Grants CAM/CSIC: CCG07-CSIC/MAT-2296, FPU AP2005-1063, and MAT2005-01,768 from MICINN, Spain. The technical support of A. Labrador and F. Fauth for X-ray scattering synchrotron measurements at BM16, European Synchrotron Radiation Facility, Grenoble, France, is gratefully acknowledged. We are also grateful to Dr. M. A. Arenas for the help in the preparation of some of the AAO templates and D. Gómez for the SEM experiments.

References and Notes

(1) Whitesides, G. M.; Boncheva, M. *Proc. Natl. Acad. Sci. U.S.A.* **2002**, *99* (8), 4769–4774.
(2) Strobl, G. *The Physics of Polymers*; Springer: Berlin, 1996.
(3) Capitan, M. J.; Rueda, D. R.; Ezquerra, T. A. *Macromolecules* **2004**, *37* (15), 5653–5659.
(4) Loo, Y.-L.; Register, R. A.; Ryan, A. J. *Phys. Rev. Lett.* **2000**, *84* (18), 4120.
(5) Hsiao, M.-S.; Chen, W. Y.; Zheng, J. X.; Van Horn, R. M.; Quirk, R. P.; Ivanov, D. A.; Thomas, E. L.; Lotz, B.; Cheng, S. Z. D. *Macromolecules* **2008**, *41* (13), 4794–4801.
(6) Zhu, L.; Cheng, S. Z. D.; Calhoun, B. H.; Ge, Q.; Quirk, R. P.; Thomas, E. L.; Hsiao, B. S.; Yeh, F.; Lotz, B. *J. Am. Chem. Soc.* **2000**, *122* (25), 5957–5967.
(7) Huang, P.; Zhu, L.; Cheng, S. Z. D.; Ge, Q.; Quirk, R. P.; Thomas, E. L.; Lotz, B.; Hsiao, B. S.; Liu, L.; Yeh, F. *Macromolecules* **2001**, *34* (19), 6649–6657.
(8) Huang, P.; Zhu, L.; Guo, Y.; Ge, Q.; Jing, A. J.; Chen, W. Y.; Quirk, R. P.; Cheng, S. Z. D.; Thomas, E. L.; Lotz, B.; Hsiao, B. S.; Avila-Orta, C. A.; Sics, I. *Macromolecules* **2004**, *37* (10), 3689–3698.
(9) Adam, G.; Gibbs, J. H. *J. Chem. Phys.* **1965**, *43* (1), 139–146.
(10) Cangialosi, D.; Alegria, A.; Colmenero, J. *Phys. Rev. E* **2007**, *76* (1), 011514.
(11) Schönhals, A.; Goering, H.; Schick, C.; Frick, B.; Zorn, R. *Colloid Polym. Sci.* **2004**, *282* (8), 882–891.
(12) Serghei, A.; Kremer, F. *Phys. Rev. Lett.* **2003**, *91* (16), 1657021–1657024.
(13) Kropka, J. M.; Garcia Sakai, V.; Green, P. F. *Nano Lett.* **2008**, *8* (4), 1061–1065.
(14) Sanz, A.; Ruppel, M.; Douglas, J. F.; Cabral, J. T. *J. Phys.: Condens. Matter* **2008**, *20* (10), 4209–4209.
(15) Bansal, A.; Yang, H. C.; Li, C. Z.; Cho, K. W.; Benicewicz, B. C.; Kumar, S. K.; Schadler, L. S. *Nat. Mater.* **2005**, *4* (9), 693–698.
(16) Alcoutlabi, M.; McKenna, G. B. *J. Phys.: Condens. Matter* **2005**, *17* (15), R461–R524.
(17) Schüller, J.; Richert, R.; Fischer, E. W. *Phys. Rev. B* **1995**, *52* (21), 15232.
(18) Napolitano, S.; Lupascu, V.; Wubbenhorst, M. *Macromolecules* **2008**, *41* (4), 1061–1063.

(19) Shin, K.; Obukhov, S.; Chen, J.-T.; Huh, J.; Hwang, Y.; Mok, S.; Dobriyal, P.; Thiyagarajan, P.; Russell, T. P. *Nat. Mater.* **2007**, *6* (12), 961–965.
(20) Zhang, M.; Dobriyal, P.; Chen, J.-T.; Russell, T. P.; Olmo, J.; Merry, A. *Nano Lett.* **2006**, *6* (5), 1075–1079.
(21) Steinhart, M. W., J.H.; Greiner, A.; Wherspohn, R. B.; Nielsch, K.; Schilling, J.; Choi, J.; Gösele, U. *Science* **2002**, 296.
(22) Steinhart, M. Supramolecular Organization of Polymeric Materials in Nanoporous Hard Templates. In *Self-Assembled Nanomaterials II; Advances in Polymer Science 220*; Springer: Berlin, 2008; pp 123−187.
(23) Shin, K.; Woo, E.; Jeong, Y. G.; Kim, C.; Huh, J.; Kim, K. W. *Macromolecules* **2007**, *40* (18), 6617–6623.
(24) Steinhart, M.; Goring, P.; Dernaika, H.; Prabhukaran, M.; Gösele, U.; Hempel, E.; Thurn-Albrecht, T. *Phys. Rev. Lett.* **2006**, *97* (2), 027801.
(25) Steinhart, M.; Senz, S.; Wehrspohn, R. B.; Gösele, U.; Wendorff, J. H. *Macromolecules* **2003**, *36* (10), 3646–3651.
(26) Woo, E.; Huh, J.; Jeong, Y. G.; Shin, K. *Phys. Rev. Lett.* **2007**, *98* (13), 136103.
(27) Hui, W.; Wei, W.; Yan, H.; Zhaohui, S. *Macromol. Rapid Commun.* **2009**, *30* (3), 194–198.
(28) Martín, J.; Mijangos, C. *Langmuir* **2009**, *25* (2), 1181–1187.
(29) Masuda, H.; Fukuda, K. *Science* **1995**, *268* (5216), 1466–1468.
(30) Li, A. P.; Muller, F.; Birner, A.; Nielsch, K.; Gosele, U. *J. Appl. Phys.* **1998**, *84* (11), 6023–6026.
(31) Rueda, D. R.; Garcia-Gutierrez, M. C.; Nogales, A.; Capitan, M. J.; Ezquerra, T. A.; Labrador, A.; Fraga, E.; Beltran, D.; Juanhuix, J.; Herranz, J. F.; Bordas, J. *Rev. Sci. Instrum.* **2006**, *77* (3), 033904.
(32) Hiroyuki Sasabe, S. S. M. A. H. K. *J. Polym. Sci., Part A-2: Polym. Phys.* **1969**, *7* (8), 1405–1414.
(33) Nogales, A.; Ezquerra, T. A.; Denchev, Z.; Sics, I.; Calleja, F. J. B.; Hsiao, B. S. *J. Chem. Phys.* **2001**, *115* (8), 3804–3813.
(34) Arndt, M.; Stannarius, R.; Groothues, H.; Hempel, E.; Kremer, F. *Phys. Rev. Lett.* **1997**, *79* (11), 2077.
(35) Schönhals, A.; Goering, H.; Schick, C. *J. Non-Cryst. Solids* **2002**, *305* (1−3), 140–149.
(36) Nogales, A.; Denchev, Z.; Sics, I.; Ezquerra, T. A. *Macromolecules* **2000**, *33* (25), 9367–9375.
(37) Kraus, J.; Müller-Buschbaum, P.; Kuhlmann, T.; Schubert, D. W.; Stamm, M. *Europhys. Lett.* **2000**, *49* (2), 210–216.
(38) Jones, R. L.; Kumar, S. K.; Ho, D. L.; Briber, R. M.; Russell, T. P. *Nature (London)* **1999**, *400* (6740), 146–149.
(39) Mukhopadhyay, M. K.; Jiao, X.; Lurio, L. B.; Jiang, Z.; Stark, J.; Sprung, M.; Narayanan, S.; Sandy, A. R.; Sinha, S. K. *Phys. Rev. Lett.* **2008**, *101* (11), 115501.
(40) Evmenenko, G.; Mo, H. D.; Kewalramani, S.; Dutta, P. *Polymer* **2006**, *47* (3), 878–882.
(41) Mischler, C.; Baschnagel, J.; Binder, K. *Adv. Colloid Interface Sci.* **2001**, *94* (1−3), 197–227.
(42) Napolitano, S.; Prevosto, D.; Lucchesi, M.; Pingue, P.; D'Acunto, M.; Rolla, P. *Langmuir* **2007**, *23* (4), 2103–2109.
(43) Ma, Y.; Hu, W. B.; Reiter, G. *Macromolecules* **2006**, *39* (15), 5159–5164.
(44) Ma, Y.; Hu, W. B.; Hobbs, J.; Reiter, G. *Soft Matter* **2008**, *4* (3), 540–543.
(45) Stribeck, N.; Buchner, S. *J. Appl. Crystallogr.* **1997**, *30* (2), 722–726.